Supplementary Information

Open-Loop Control of Soft Hydrogel Microrobot Swarms for Targeted Thrombolysis in a Preclinical Model

Yimo Y. Yan[1,#], Joshua M. Mesfin[1,2,#], Tim Grossrieder[1], Gian-Andrea Burkard[1], Archit Mundada[1], Myungjin Park[1], Laurensz Moeharram[1], Zaiyi Shen[3], Dongfang Fu[3], Louise Gillion[1], Petra Wolint[2], Christian T. Stoeck[4], Jianbo Tang[1], Etienne Geistlich[1], Arthur Vermeersch[1], Stella Morger[1], Nikola Cesarovic[2,5,6], Simone Schuerle[1,*]

1 Institute of Robotics and Intelligent Systems, Department of Health Sciences and Technology, ETH Zurich, 8092 Zurich, Switzerland

2 Institute of Translational Medicine, Department of Health Sciences and Technology, ETH Zurich, 8092 Zurich, Switzerland

3 State Key Laboratory for Turbulence and Complex Systems, School of Mechanics and Engineering Science, Peking University, Beijing, China

4 Center for Preclinical Development, University Hospital of Zurich, University of Zurich, Zurich, Switzerland

5 Deutsches Herzzentrum der Charité (DHZC), Department of Cardiothoracic and Vascular Surgery, Berlin, Germany

6 Charité – Universitätsmedizin Berlin, corporate member of Freie Universität Berlin and Humboldt-Universität zu Berlin and Berlin Institute of Health, Berlin, Germany

[#] These authors contributed equally and are listed in no particular order, to be regarded as co-first authors.

*Corresponding author: Simone Schuerle

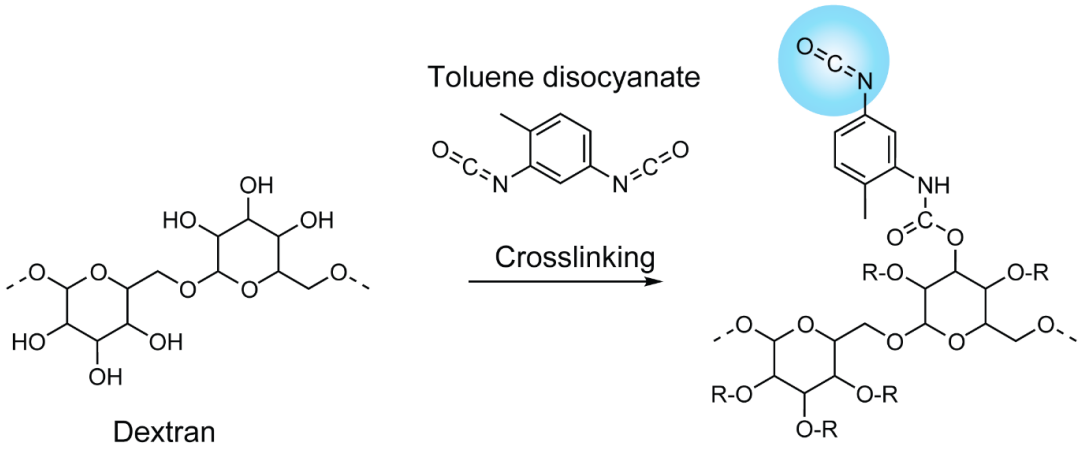

Supplementary Information Figure 1. Chemical Reaction of Toluene Diisocyanate (TDI) Crosslinking. Dextran, in the presence of TDI, crosslinks when as the water-in-oil precursor magnetic droplet. The polyaddition reaction is further facilitated under an external magnetic field produced by a Rotating Halbach Cylinder device.

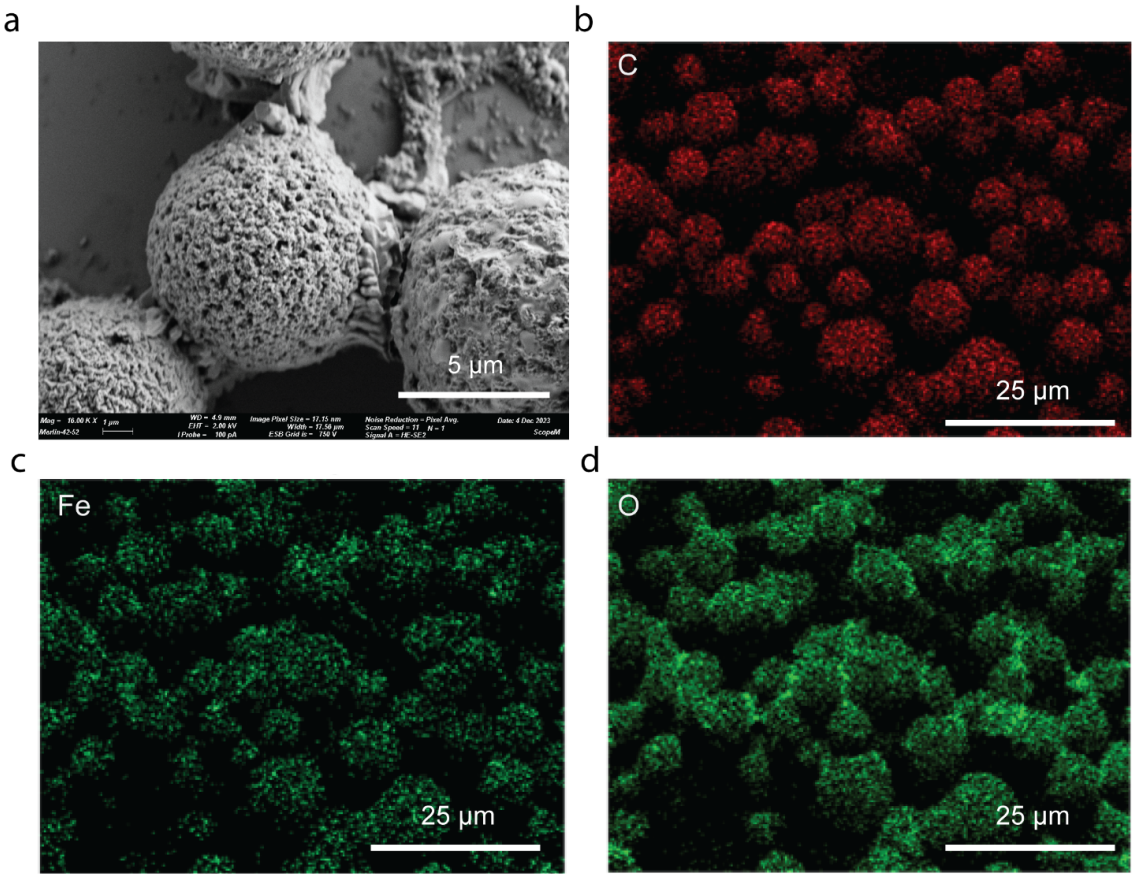

Supplementary Information Figure 2. Scanning Electron Microscopy (SEM) and Structural Analysis of Homogenous Microrobots. (a) SEM image of homogenous microrobots. Scale bar: 5 µm. **(b-d)** EDX images of homogenous microrobots, with coverage of carbon **(b)**, iron **(c)**, and oxygen **(d)**. Scale bar: 25 µm.

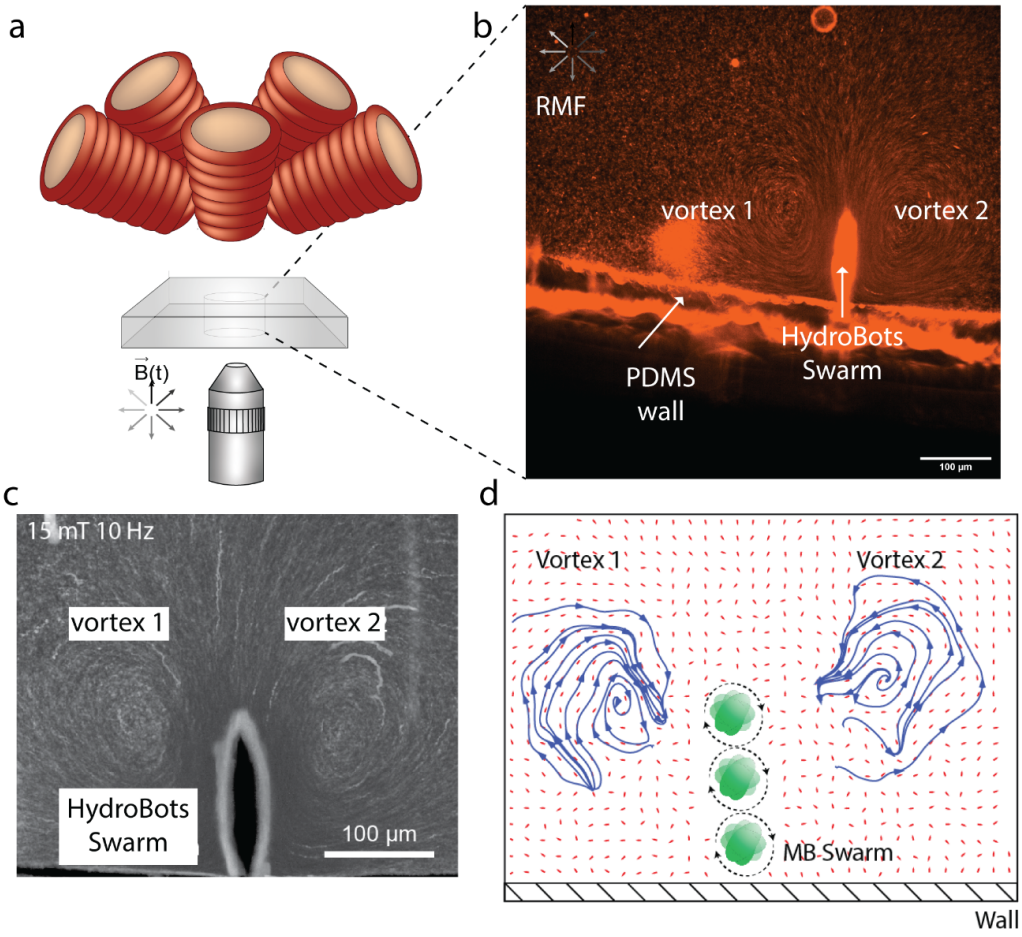

Supplementary Information Figure 3. Swarm Behavior Characterization. (a) Schematic of PDMS microfluidic ring placed in the working space of an MFG-100-i. **(b)** Vortex formation induced by rotating HydroBots swarm visualized by Cy3 nanoparticles. Scale bar: 100 µm. **(c)** PIV analysis of HydroBot swarm behavior. Scale bar: 100 µm. **(d)** PIV result. Streamlines of the convection flow induced by the rotating HydroBot swarm.

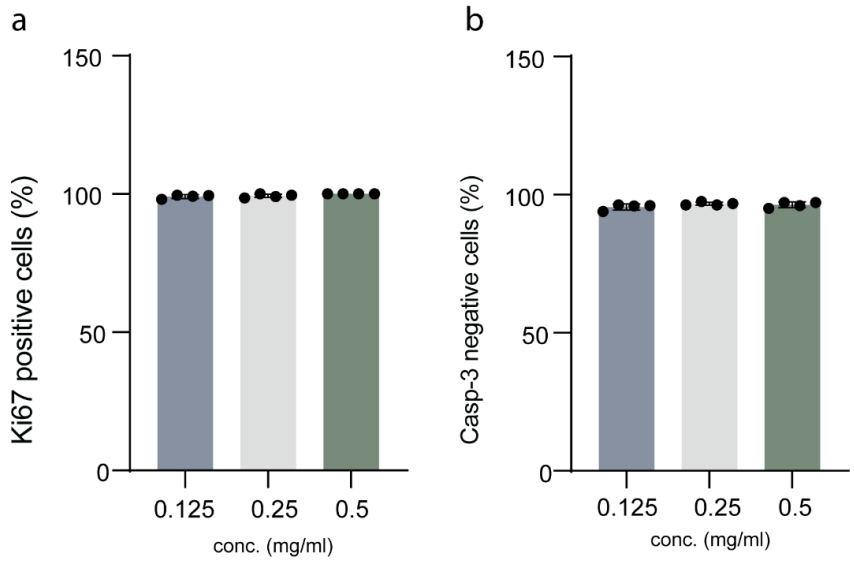

Supplementary Information Figure 4. Endothelial Cell Proliferation and Minimal Cell Death with HydroBot Administration. (a-b) HMEC-1 cells that were treated with various HydroBot concentrations (0.125, 0.25, 0.5 mg/mL) for 24 hours were thus stained for cleaved caspase 3 **(a)** and Ki-67 **(b)**. N = 4 replicates for each condition.

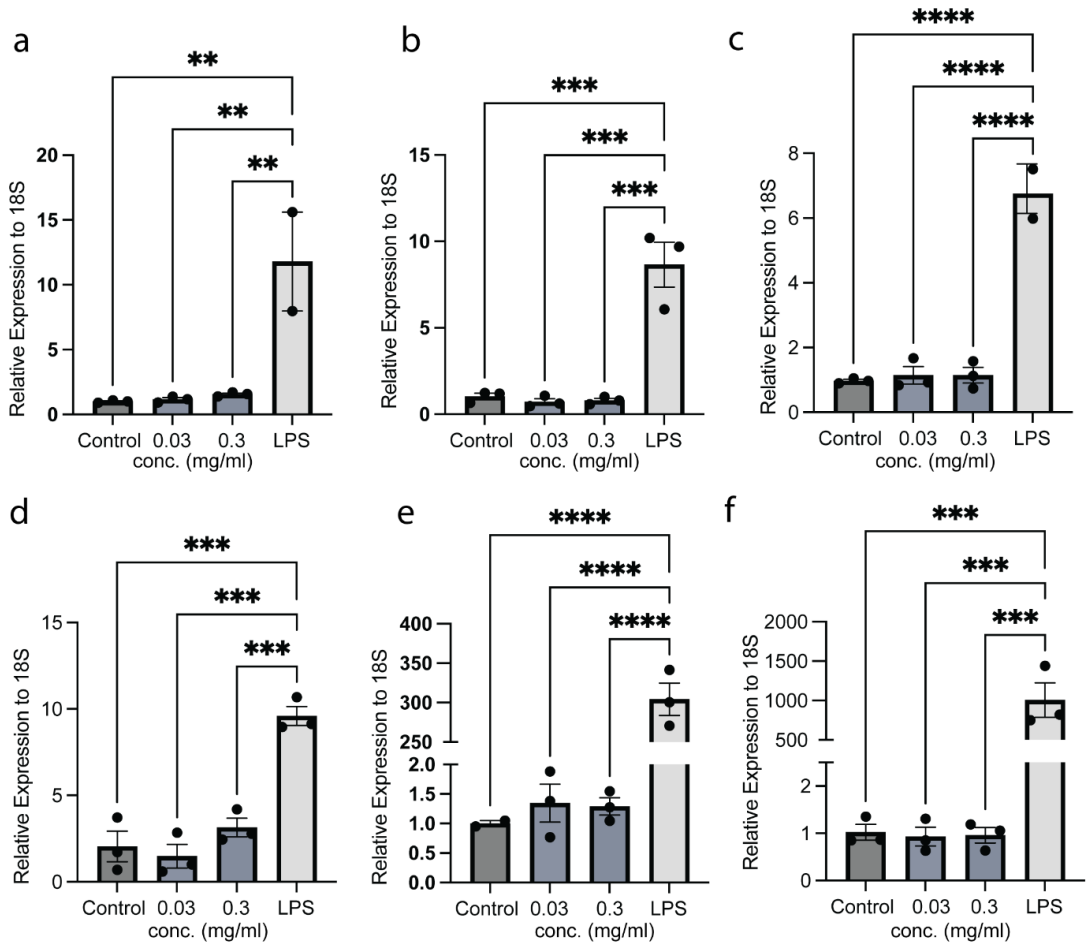

Supplementary Information Figure 5. qPCR Immunogenicity on THP-1 Macrophages. (a-c) IL-1β **(a),** IL-6 **(b)**, and TNF-α **(c)** expression from THP-1 derived macrophages that were treated with either PBS, 0.3 mg/mL HydroBots, 0.03 mg/mL HydroBots, and 1 µg/mL lipopolysaccharide for 24 hours. **(d-f)** IL-1β **(d),** IL-6 **(e)**, and TNF-α **(f)** expression from THP-1 derived macrophages that were treated with either PBS, 0.3 mg/mL HydroBots, 0.03 mg/mL HydroBots, and 1 µg/mL lipopolysaccharide for 48 hours.

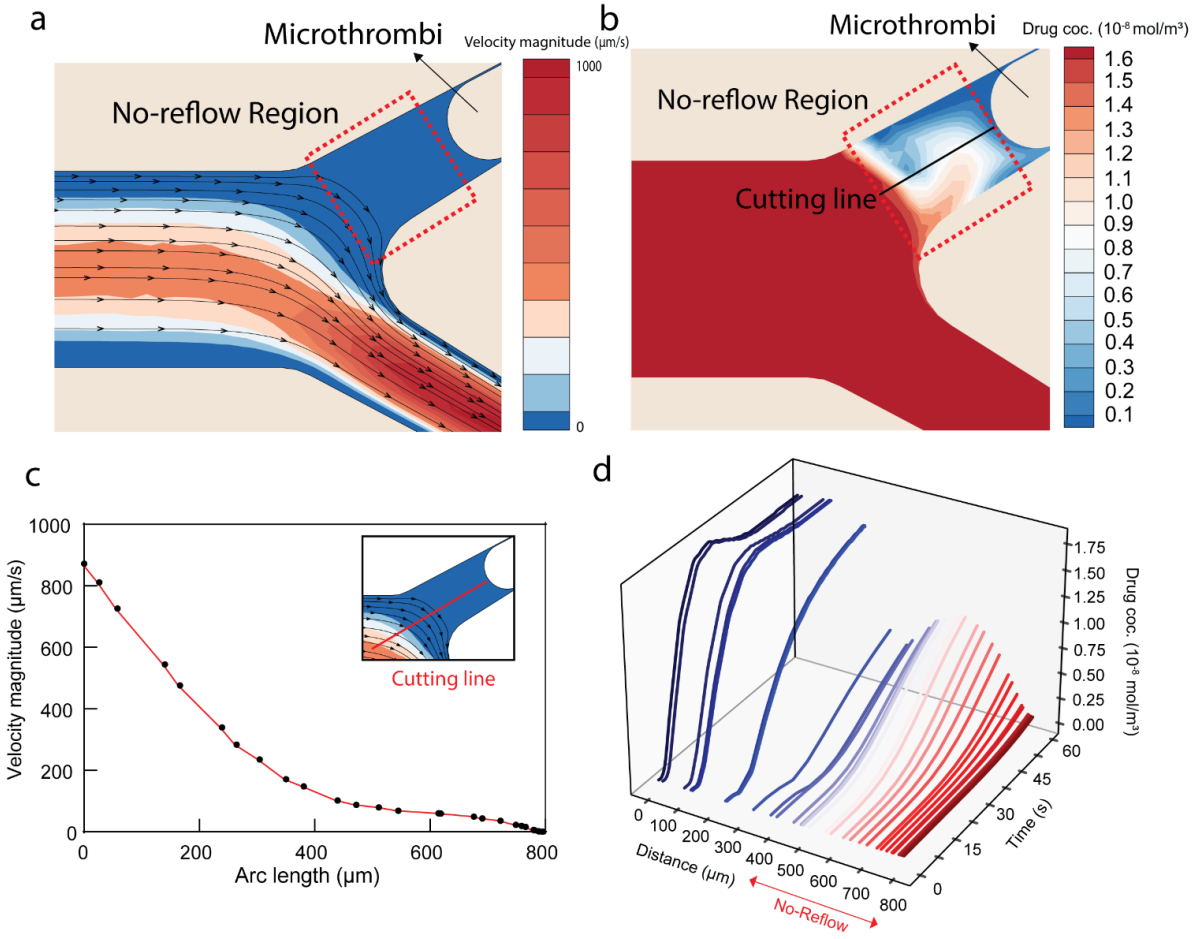

Supplementary Information Figure 6. Modelling the No-Reflow Region. **(a)** Simulated flow velocity profile within the no-reflow region. **(b)** Simulated drug infiltration pattern into the no-reflow region. **(c)** Flow velocity gradually decreases along the designated cutting line in the no-reflow region. **(d)** Temporal changes in drug concentration measured along the same cutting line within the no-reflow region.

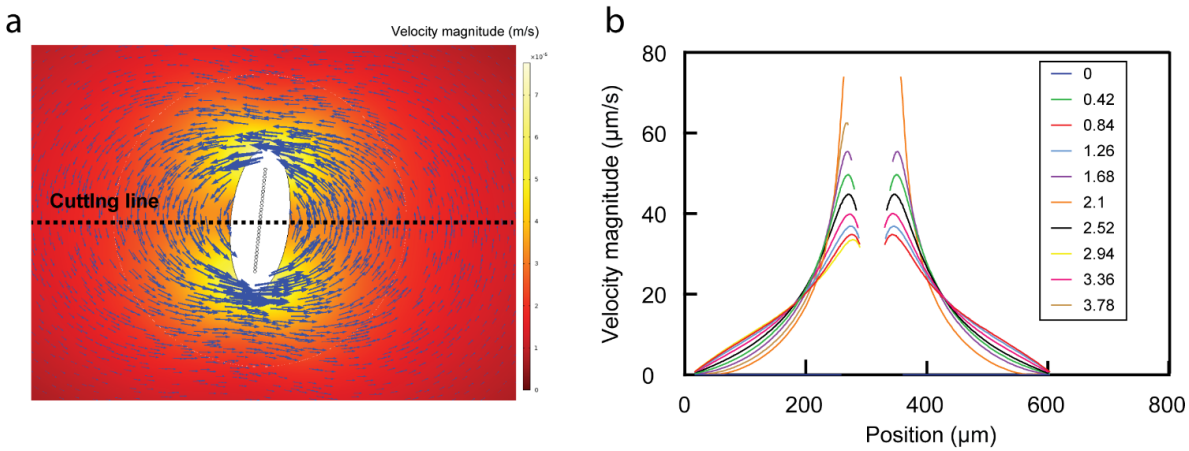

Supplementary Information Figure 7. Modelling Convection Flow Induced by HydroBot . (a) Induced convection flow by rotating HydroBots. **(b)** Velocity magnitude along the cutting line.

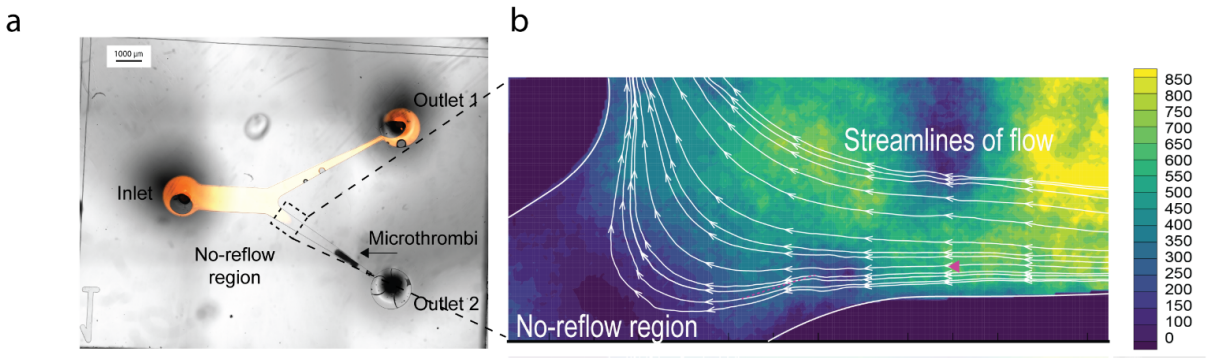

Supplementary Information Figure 8. Velocity Profile of No-Reflow Microfluidic Chip. (a) PIV analysis depicting the velocity profile characteristic of the no-reflow region. **(b)** Microfluidic chip design of the no-reflow region.

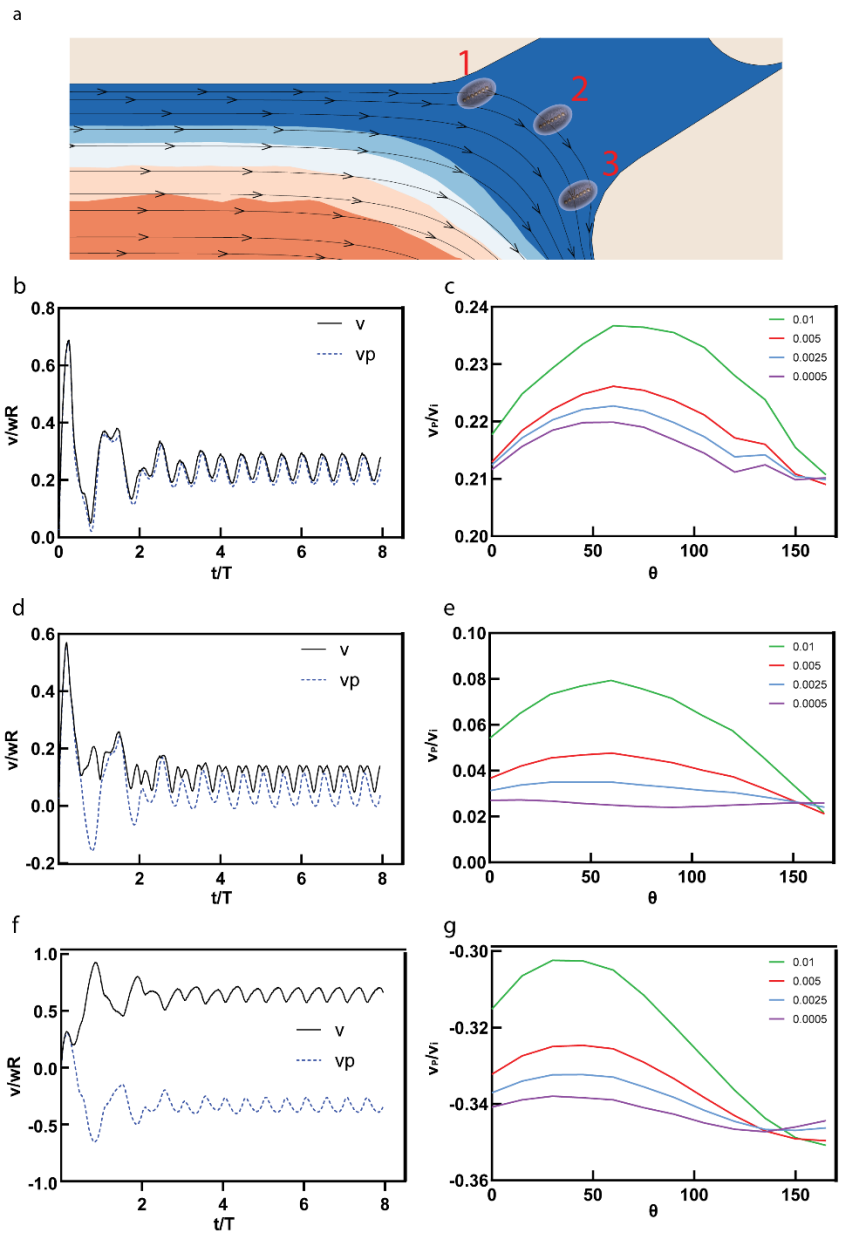

Supplementary Information Figure 9. Computational Modeling of Interactions with HydroBot in the No-reflow Region. **(a)** Positions of HydroBots (1–3) used for simulation in the no-reflow region. **(b)**Time-dependent variation of HydroBot's velocity at position 1. **(c)** HydroBot's velocity along the channel at position 1 for different driving frequencies. **(d)** Time-dependent variation of HydroBot's velocity at position 2. **(e)** HydroBot's velocity along the channel at position 2 for different driving frequencies. **(f)** Time-dependent variation of HydroBot's velocity at position 3. **(g)** HydroBot's velocity along the channel at position 3 for different driving frequencies.

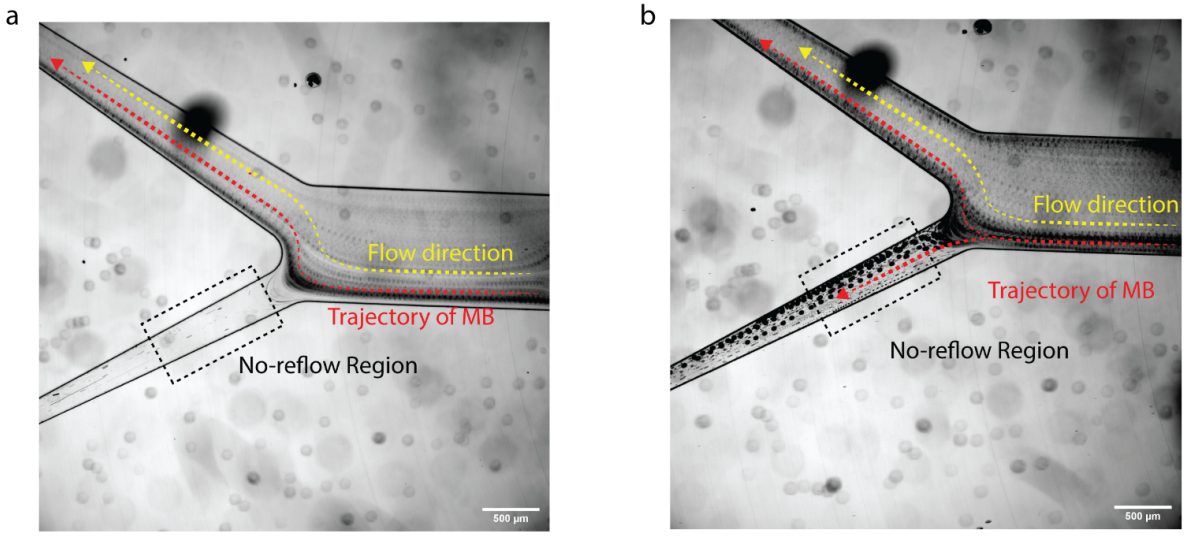

Supplementary Information Figure 10. Time-lapse of Homogeneous Microrobots Steered into No-Reflow Region. (a) Time-lapse images showing homogeneous microrobots drifting with the flow and bypassing the no-reflow region. Scale bar: 500 µm. **(b)** Time-lapse images of part of the homogenous microrobots adjacent to the no-reflow region being steered into the no-reflow region. Scale bar: 500 µm.

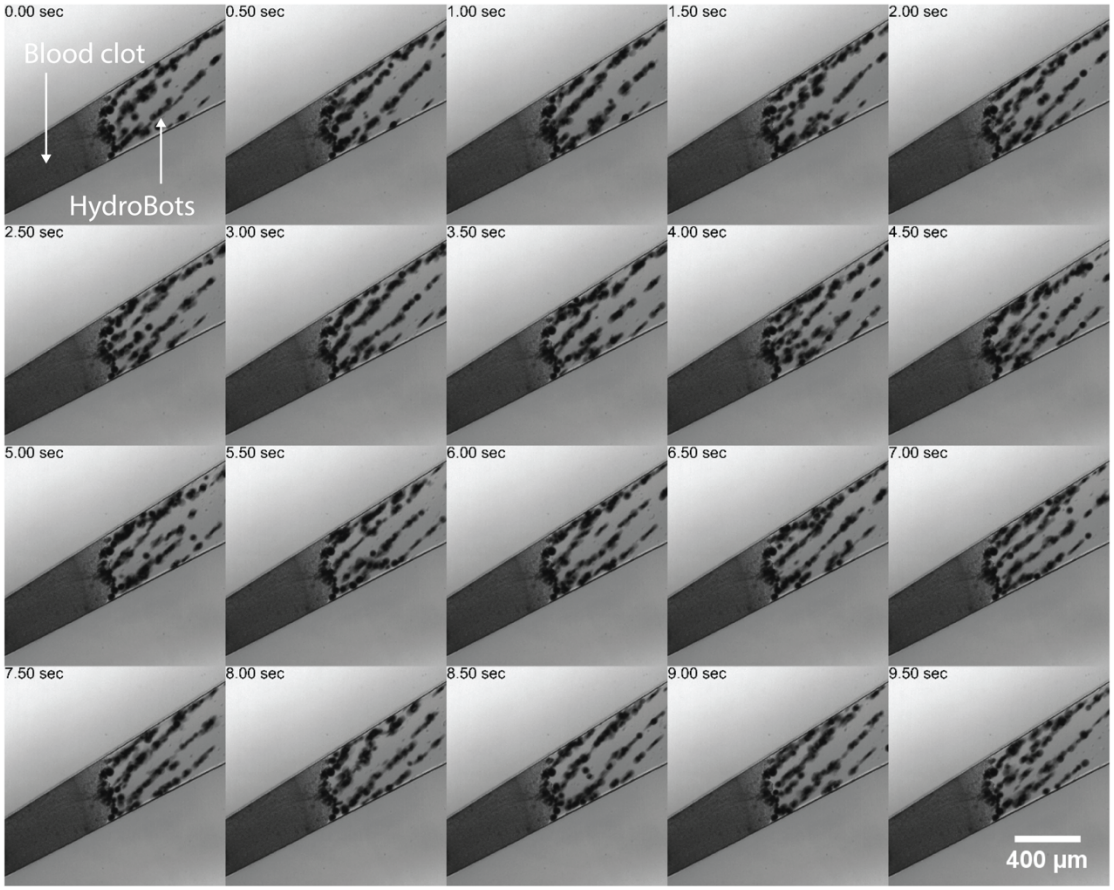

Supplementary Information Figure 11. HydroBots Without Thrombolytics Cannot Induce Thrombolysis. Time series images of HydroBots attempting to break down the blood clot. Scale bar: 400 µm.

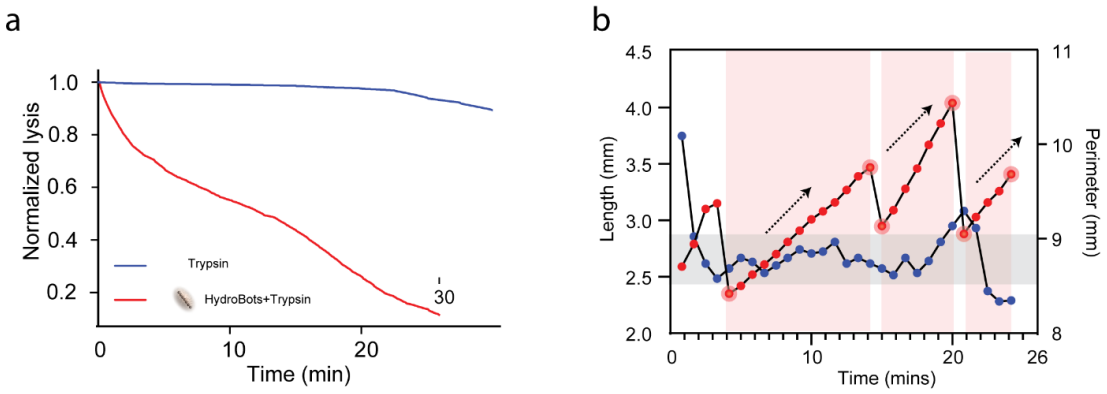

Supplementary Information Figure 12. HydroBots Induce Thrombolysis with Trypsin. (a) Normalized lysis area with 0.25% trypsin alone (blue) vs. HydroBots (5 mg/mL) with 0.25% trypsin (red). HydroBots and trypsin achieve lysis within 27 minutes. **(b)** The length (red) increases between drug and clot with HydroBot addition, leading to higher contact area for thrombolysis. The perimeter of the blood clot (blue) remains the same.

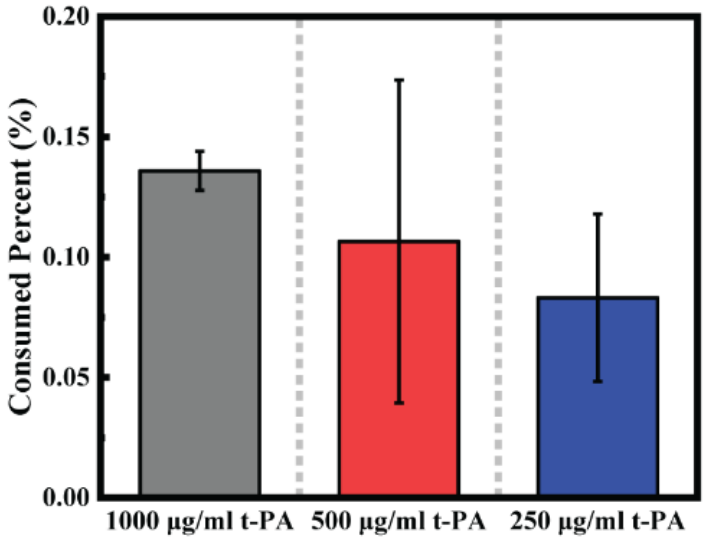

Supplementary Information Figure 13. tPA Comparisons. Relative clot areas as consumed percentages for 250 µg/mL, 500 µg/mL, and 1000 µg/mL t-PA over the course of 40 minutes of lysis.

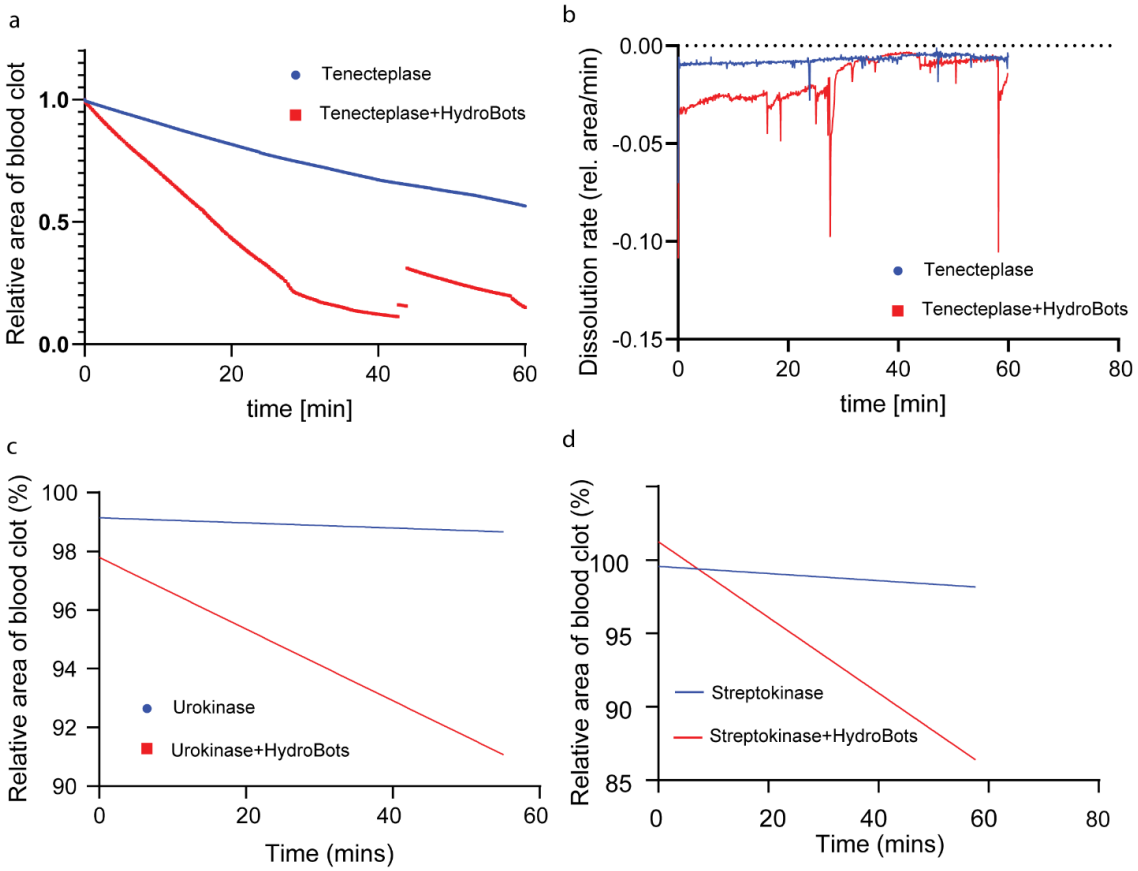

Supplementary Information Figure 14. HydroBots Induce Thrombolysis with Other Thrombolytic Agents. (a-b) HydroBots (10mg/mL) with Tenecteplase (1 mg/mL) demonstrate better thrombolysis relative to Tenecteplase alone **(a)**, with a much higher degradation rate **(b)**. N = 3 per group. **(c)** HydroBots (10mg/mL) with urokinase (500 µg/mL) demonstrate better thrombolysis relative to urokinase alone. N = 3 per group. **(d)** HydroBots (10mg/mL) with streptokinase (500 µg/mL) demonstrate better thrombolysis relative to streptokinase alone N = 3 per group.

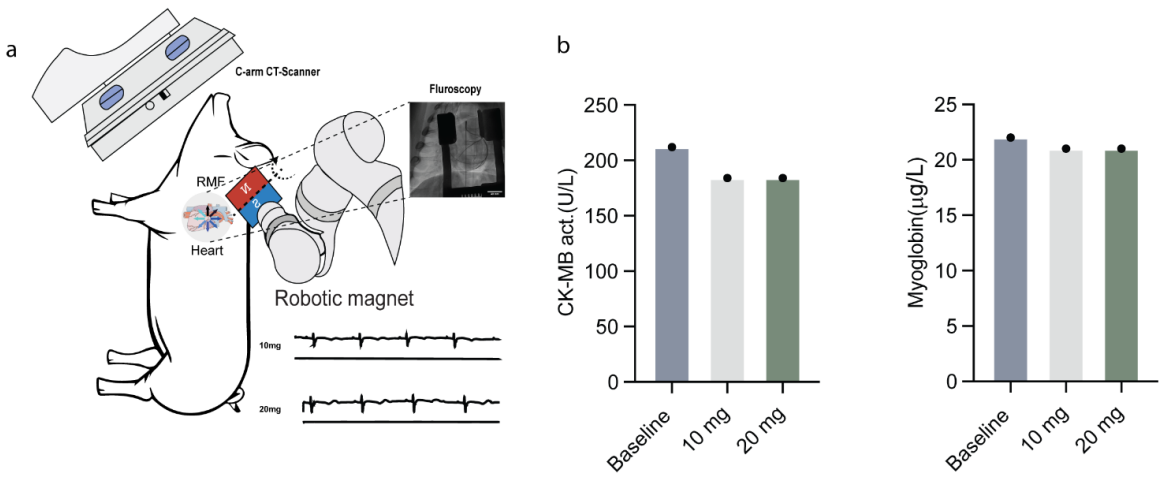

Supplementary Information Figure 15. Cardiac Safety HydroBot Study. (a) Overview of the cardiac study with an external rotating magnet over the heart. Both 10 mg and 20 mg of HydroBots were administered via intracoronary infusion. Electrocardiogram data suggest no difference with microrobot administration. **(b)** Creatine kinase MB (CK-MB) and myoglobin did not increase in response to HydroBot administration.

a

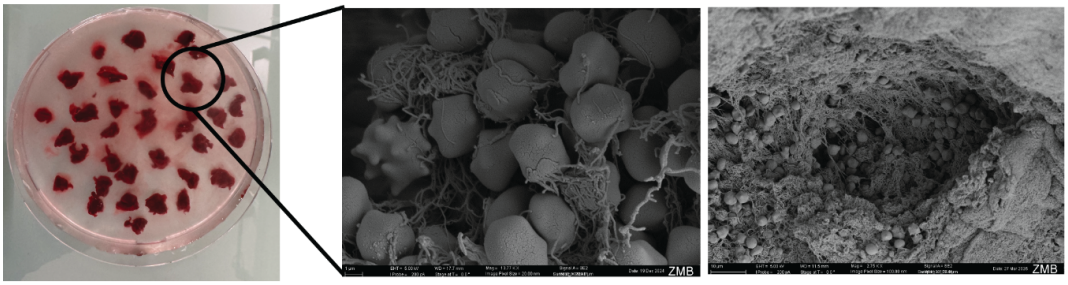

b

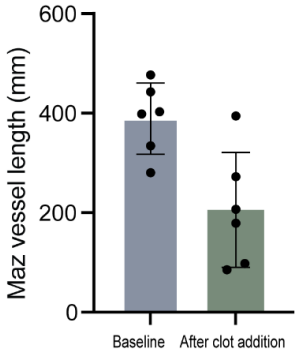

Supplementary Information Figure 16. Blood Clot Size Validation and Maximum Vessel Length Validation. (a) Porcine blood clots created ex vivo. Scale bar: 1 cm. Scanning electron microscope (SEM) image of porcine blood clot. **(b)** Using AI-enhanced analysis, we quantified the maximum vessel length at baseline before clot introduction vs. the maximum vessel length of the vessel post-occlusion.

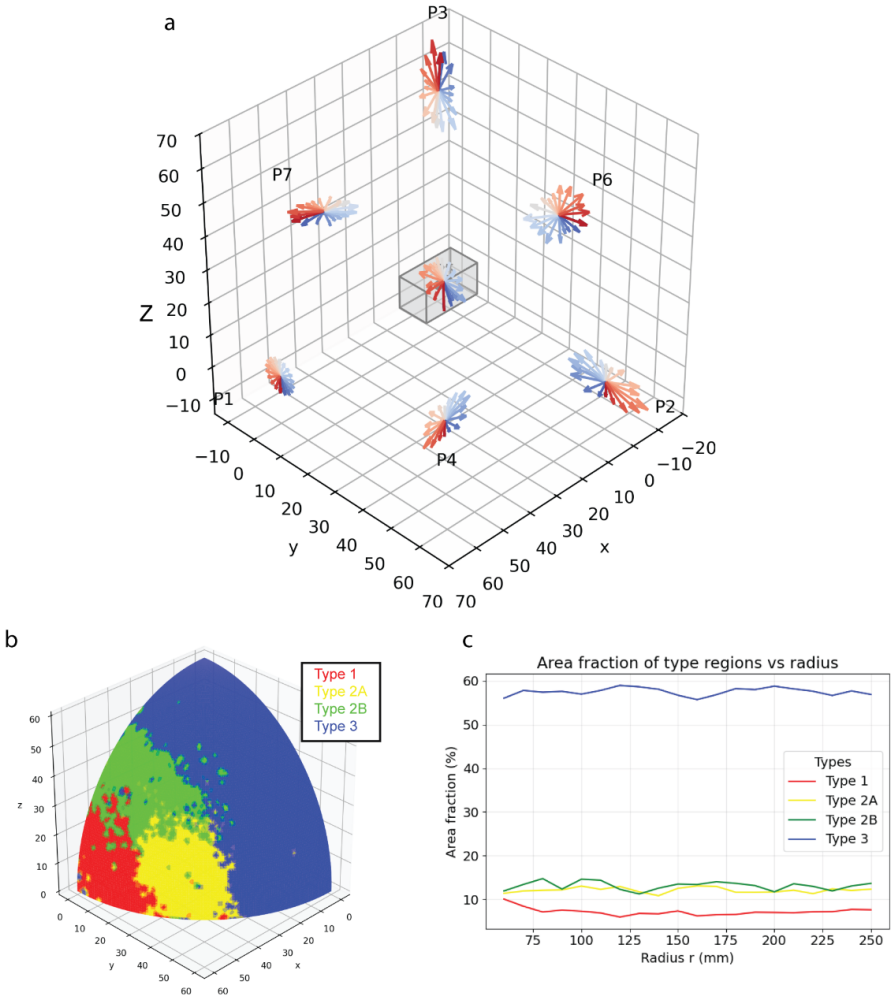

Supplementary Information Figure 17. Magnetic Field Simulation. (a) RMF produced by a magnet at (0,0,0) rotating around the positive x-axis at different positions in space. **(b)** Octant of radius 60 mm with magnet centered at (0, 0, 0) divided into four regions based on the direction of the rotation axis relative to the x-axis. Type 1 RMF has a rotation axis with a max offset of 60° from the positive x-axis, Type 2A and 2B RMF have a rotation axis with an offset between 60° and 120° from the positive x-axis, and Type 3 RMF has a rotation axis with a max offset of 60° from the negative x-axis, **(c)** Area fraction of each RMF in the octant with varying radius.

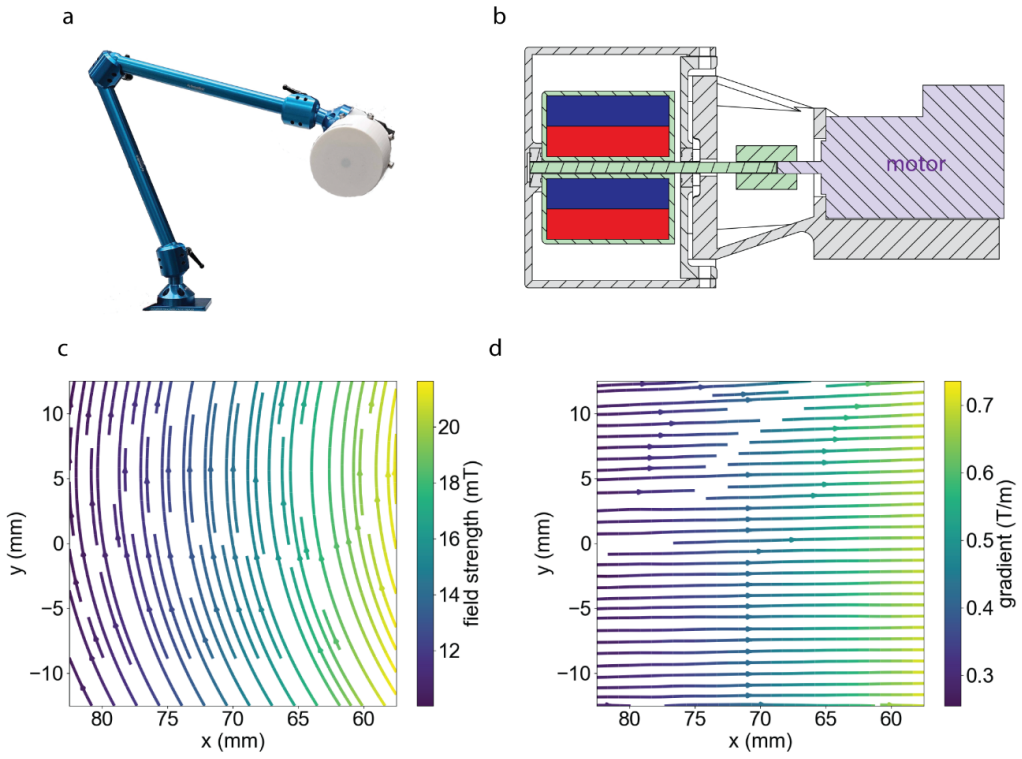

Supplementary Information Figure 18. Characterization of Magnetic Setup for *In Vivo* Trials. (a) Rotating permanent magnet mounted on a mechanical arm. **(b)** Schematic of the rotating magnet setup. Two 50.8mm x 50.8mm x 25.4mm are mounted in series around a shaft connected to the DC motor. **(c-d)** Magnetic field strength and gradient of the rotating magnet. The depicted region is shown for a distance of around 7 cm from the surface of the setup.

a

b

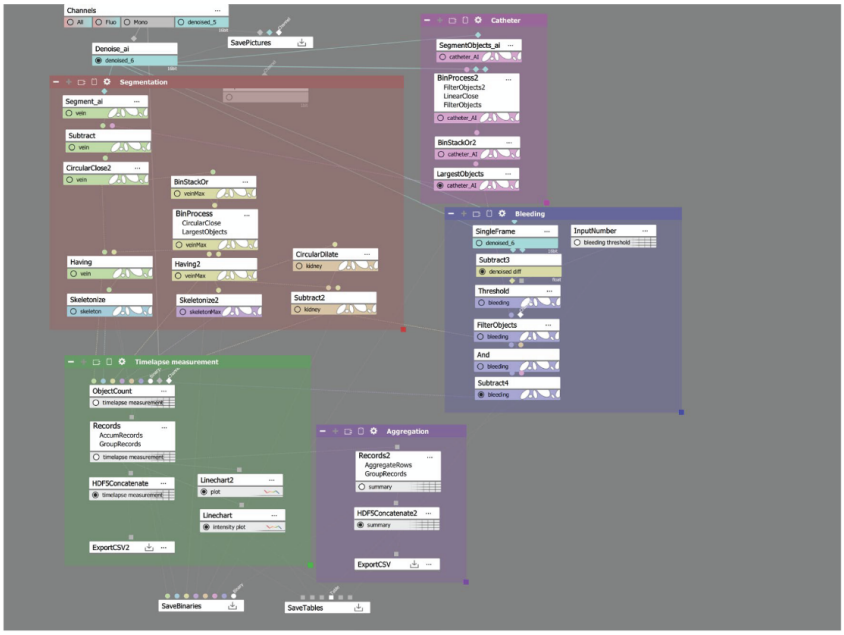

Supplementary Information Figure 19. Overview of Magnetic Setup Placement and Fluoroscopy AI-Driven Analysis. (a) Position of the magnetic arm over the porcine's HydroBot-treated kidney. **(b)** Overview of AI-driven automated analysis of fluoroscopy videos.

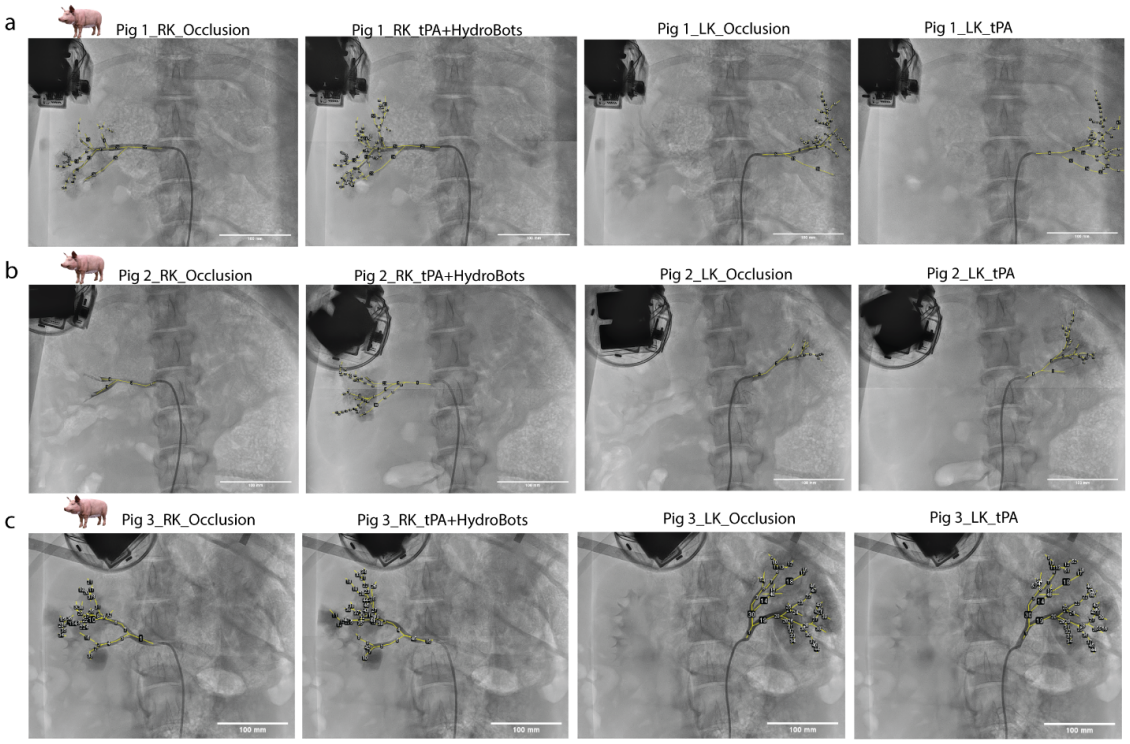

Supplementary Information Figure 20. Maximum Vessel Length Segmentation for All Animals. (b) Animal 1 with both kidneys and at both timepoints. **(c)** Animal 2 with both kidneys and at both timepoints. **(d)** Animal 3 with both kidneys and at both timepoints. Scale bar: 100 mm.

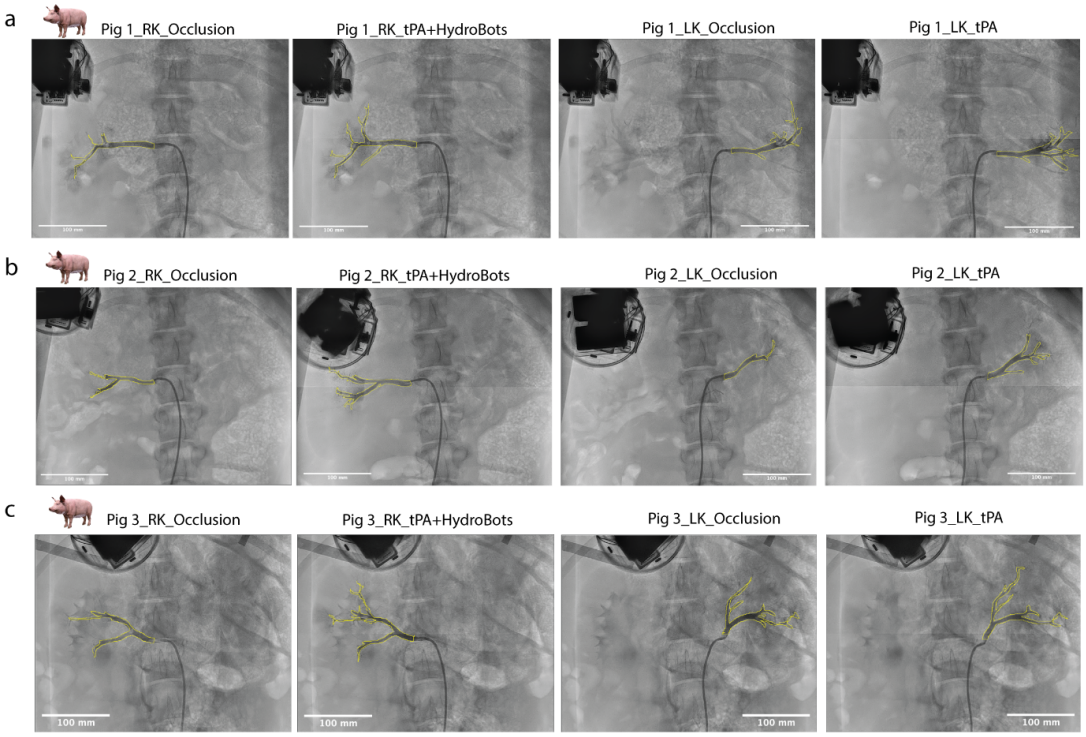

Supplementary Information Figure 21. Vessel Segmentation for All Animals. (a) Animal 1 with both kidneys and at both timepoints. **(b)** Animal 2 with both kidneys and at both timepoints. **(c)** Animal 3 with both kidneys and at both timepoints. Scale bar: 100 mm.

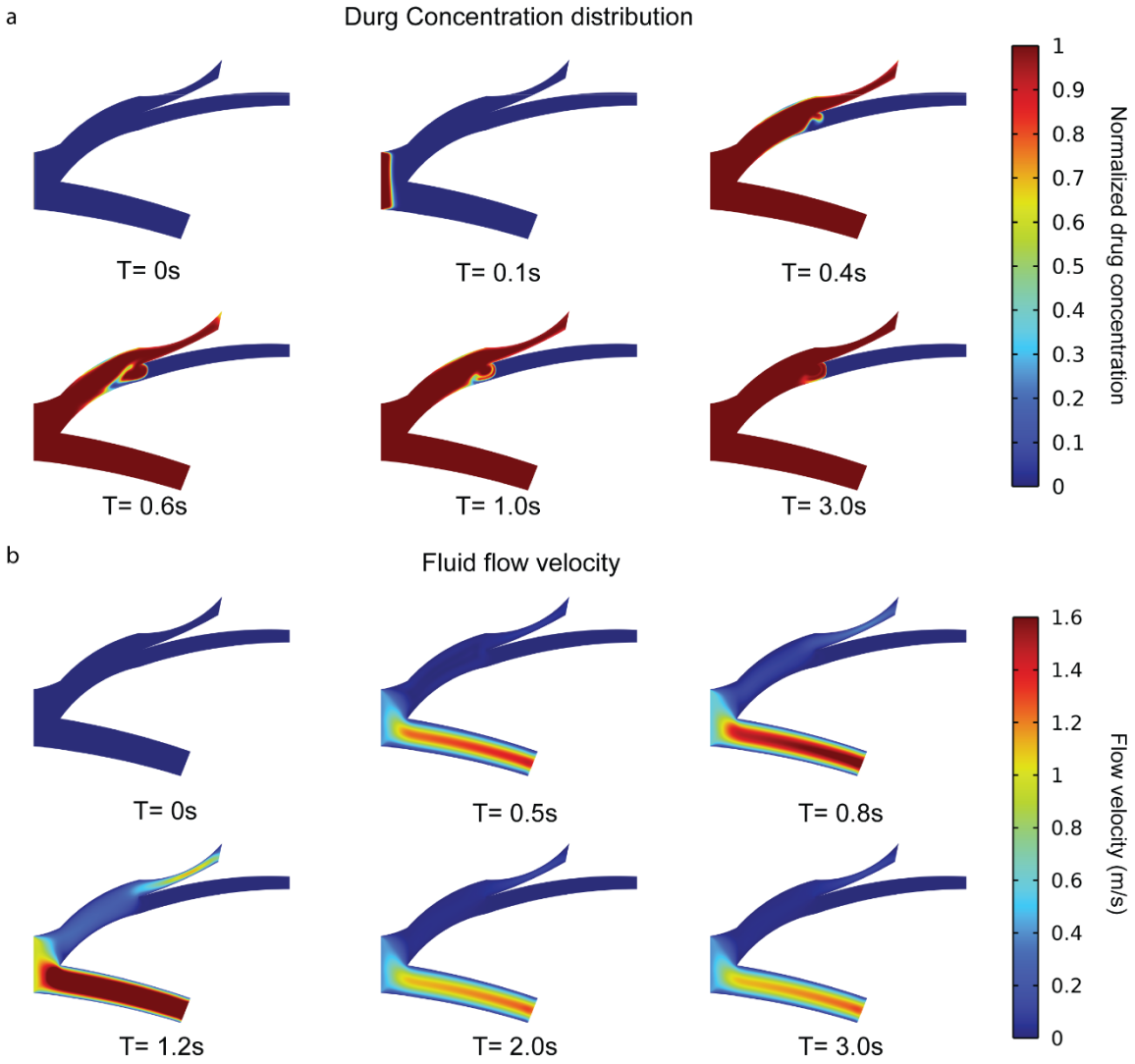

Supplementary Information Figure 22. Time-lapse Images of Drug Concentration and Flow Field Profiles. (a-b) The drug concentration **(a)** and flow field **(b)** profiles within the control group (-Hydrobot). Drugs administered via the catheter disperse primarily along the fluid flow. However, in no-flow regions, drug distribution relies solely on nature diffusion properties. The flow field exhibits pulsatile characteristics, with velocities varying over time, and is present throughout all areas except for the designated no-flow regions.

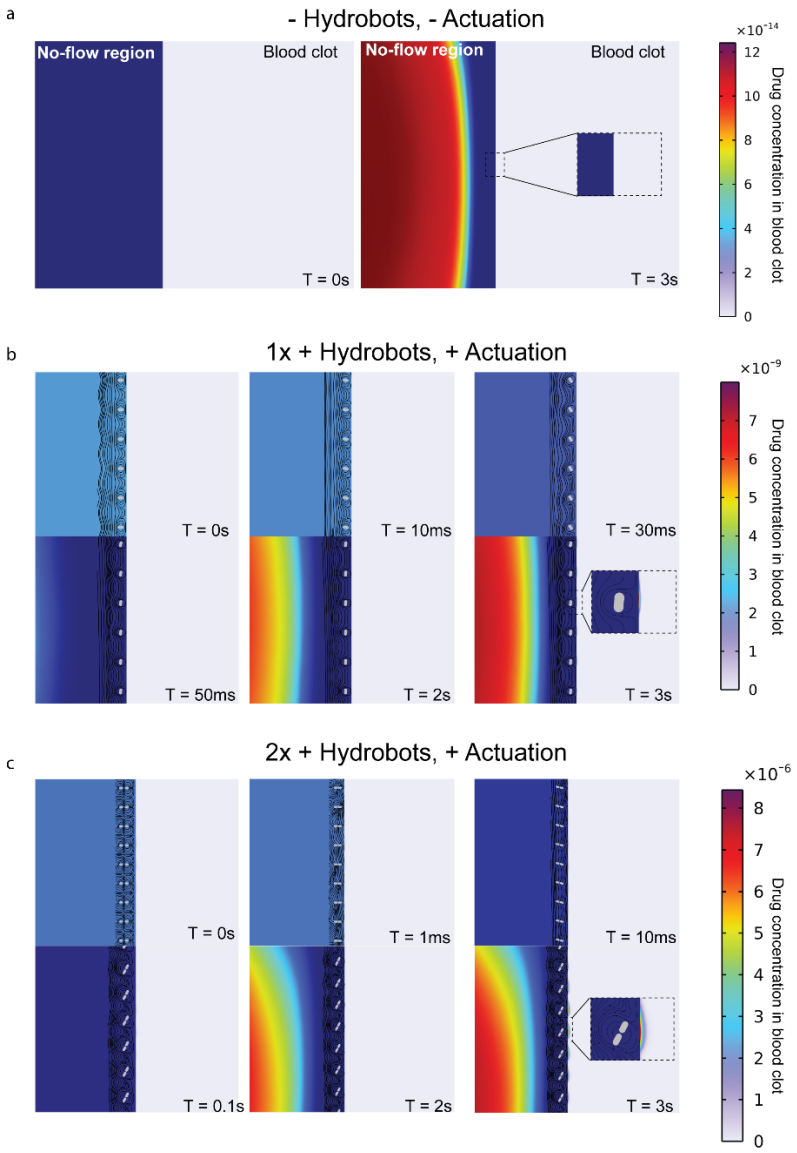

Supplementary Information Figure 23. Time-lapse Images of Drug Concentration Under the Different Groups. (a) In the control group (no HydroBots, no actuation), drug entry into the no-flow region is limited to diffusion, with minimal penetration into the blood clot. **(b)** Conversely, in the (+ 1x conc. HydroBots, with RMF actuation) group, the HydroBots rotate clockwise, creating a local flow field (indicated by black streamlines). This results in higher drug concentrations within the clot compared to the control. **(c)** In the (+ 2x conc. HydroBots, with RMF actuation) group, HydroBots form long chains due to dipole interactions. During actuation, the magnetic torque overcomes viscous torque, maintaining the assembly. The resulting hydrodynamic coupling enhances local convection, leading to even greater drug penetration than the 1x group, suggesting that higher HydroBots concentrations accelerate the treatment of blood clots.

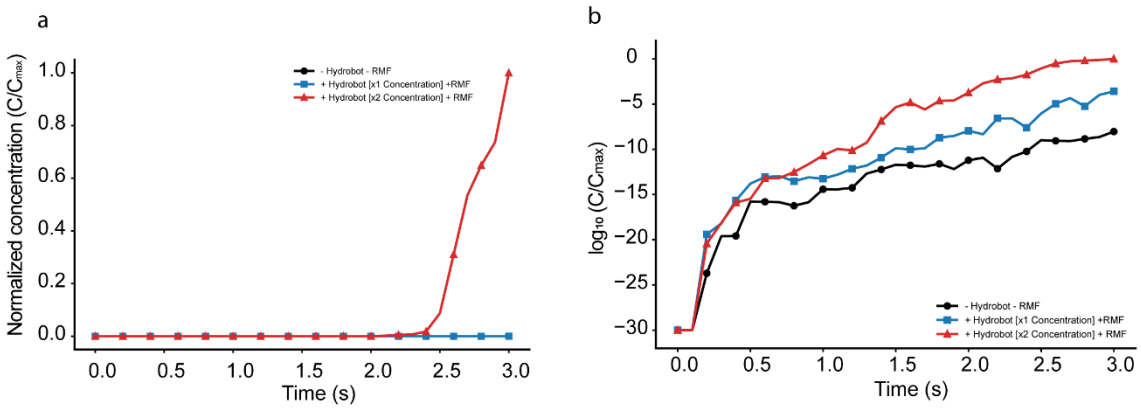

Supplementary Information Figure 24. Simulations Comparing Drug Concentration Penetration into Blood Clot. (a-b) The normalized **(a)** and log-scale normalized **(b)** average drug concentration within the blood clot. Concentrations were measured along a line 100 μm from the clot boundary to account for simulation time constraints. While initial concentrations are similar across all groups, the disparity increases significantly over time. These results demonstrate that the RMF of the HydroBots effectively drives drug diffusion into the blood clot through convective-enhanced drug delivery.

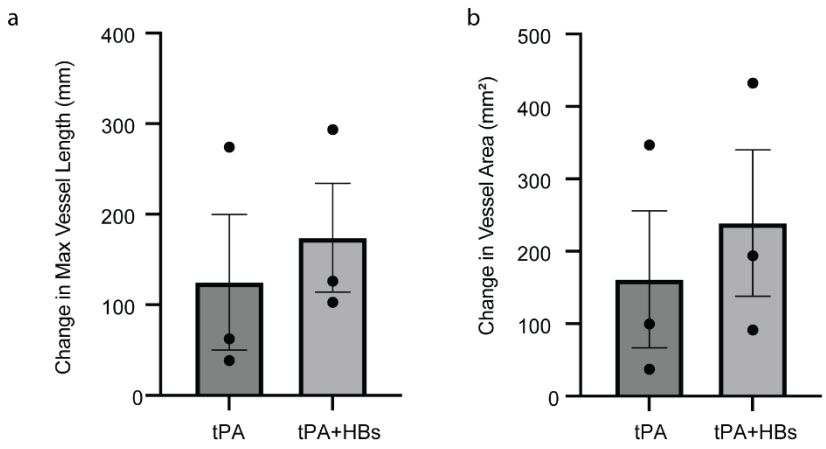

Supplementary Information Figure 25. Dose Response Recanalization. (a) Change in vessel length between 30 min post treatment and occlusion with 1.5 mg t-PA. **(b)** Change in vessel area between 30 min post treatment and occlusion with 1.5 mg t-PA.

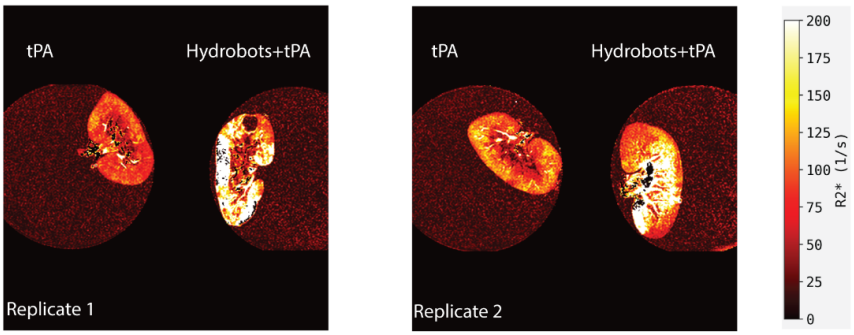

Supplementary Information Figure 26. Kidney HydroBot Distribution. R2 enhanced overview of kidneys treated with 100 mg of HydroBot plus 15 mg t-PA compared with kidneys treated with 15 mg t-PA alone.

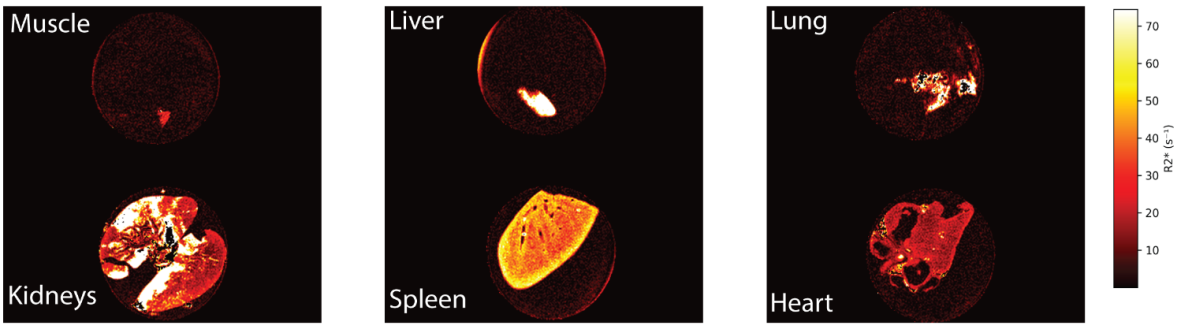

Supplementary Information Figure 27. Satellite Organ Biodistribution. R2* enhanced overview of kidneys treated with 100 mg of HydroBot plus 15 mg t-PA compared with kidneys treated with 15 mg t-PA alone, alongside biopsies of muscle, spleen, liver, lung and heart.

Supplementary Table 1. Parametric Values for Non-Newtonian Constitutive Equations

Parameters	Values
Zero shear rate viscosity limit (μ_0)	56 [cP]
Infinite shear rate viscosity limit (μ_∞)	3.5 [cP]
Relaxation time constant (λ)	3.313 [s]
Power low index in Carreau model (n)	0.3568
Artery average flow speed $\left(\underline{V}_{flow}\right)$	60 [cm/s]
Wave amplitude (A)	20 [cm/s]

Supplementary Table 2. Parametric Values for HydroBot Convection Motion Equations

Parameters	Values
Length of easy axis of microrobots (a)	20 [μm]
Length of hard axis of microrobots (b)	10 [μm]
Magnetic moment of microrobots (m)	21.2 [nAm^2]
Rotating magnetic field strength (B_0)	10 [mT]
Actuation frequency (f)	10 [Hz]
Cut out distance (R_c)	0.53a
Balance coefficient between dipole force and repulsive force (ξ)	30